Monthly Notices
of the
ROYAL ASTRONOMICAL SOCIETY

MNRAS **437,** 3112–3123 (2014)
Advance Access publication 2013 December 5

doi:10.1093/mnras/stt2048

Structure of advection-dominated accretion discs with outflows: the role of toroidal magnetic fields

A. Mosallanezhad,[1,2⋆] S. Abbassi[3,4⋆] and N. Beiranvand[5⋆]

[1]*Key Laboratory for Research in Galaxies and Cosmology, Shanghai Astronomical Observatory, Chinese Academy of Sciences, 80 Nandan Road, Shanghai 200030, China*
[2]*University of Chinese Academy of Sciences, 19A Yuquan Road, Beijing 100049, China*
[3]*Department of Physics, School of Sciences, Ferdowsi University of Mashhad, Mashhad, 91775-1436, Iran*
[4]*School of Astronomy, Institute for Research in Fundamental Sciences (IPM), PO Box 19395-5531, Tehran, Iran*
[5]*School of Physics, Damghan University, PO Box 36715-364, Damghan, Iran*

Accepted 2013 October 21. Received 2013 October 21; in original form 2013 June 13

ABSTRACT

The main aim of this article is to study the effect of toroidal magnetic fields on the structure of advection-dominated accretion flows (ADAFs) in the presence of turbulence viscosity and diffusivity due to viscosity and magnetic field respectively. We use the self-similar assumption in the radial direction to solve the magnetohydrodynamic equations for a hot accretion disc. We use spherical coordinates (r, θ, φ) to solve our equation. The toroidal component of magnetic field is considered and all three components of the velocity field $\boldsymbol{v} \equiv (v_r, v_\theta, v_\varphi)$ are present in our work. We reduce the equations to a set of differential equations in θ and apply a symmetric boundary condition at the equatorial plane of the disc. Our results indicate that the outflow region, where the radial velocity becomes positive at a certain inclination angle θ_0, always exists. The results illustrate that the stronger the magnetic field, the smaller the inclination angle θ_0 becomes. This means that a magnetized disc is thinner compared with a non-magnetized disc. According to the work of Jiao & Wu, we can define three regions. The first is called the inflow region, which starts from the disc mid-plane and extends to a certain inclination θ_0 where $v_r(\theta_0) = 0$. In this region, the velocity has a negative value and the accretion material moves towards the central object. The outflow region, where $v_r(\theta) > 0$, is placed between θ_0 and the surface of the disc, $\theta_0 < \theta < \theta_s$. In this area, the accretion flow moves away from the central object. The third region, which is located between the surface of the disc and the polar axis, is called the wind region. This area is very narrow and material is blown out from the surface in the form of wind. In this article, we consider two parameters to illustrate the magnetic field effects. These parameters are the ratio of gas pressure to magnetic pressure in the equatorial plane of the disc, β_0, and also the magnetic diffusivity parameter, η_0. Numerical calculations with our model have revealed that the toroidal component of magnetic field has a significant effect on the vertical structure of an accretion disc.

Key words: accretion, accretion discs – black hole physics – MHD – stars: winds, outflows.

1 INTRODUCTION

There has been rapid progress in understanding accretion processes in astrophysics during the past three decades. Today, we know that accretion discs exist in many astrophysical systems such as active galactic nuclei (AGN) and close X-ray binary systems (XBs), where the accretion disc surrounds a black hole.

Many theoretical models have been proposed. One of them is the standard accretion disc model presented by Shakura & Sunyaev (1973). In this model, the disc is assumed to be geometrically thin ($H/r \ll 1$) and optically thick in the vertical direction and the accreting matter moves with nearly Keplerian velocity. This model explains most of the observational features of X-ray binaries and active galactic nuclei in a highly convincing manner. However, standard disc models cannot reproduce high-energy emission such as X-ray and gamma-ray spectra. One of the most important processes that is not considered in the standard accretion disc model is advective cooling. In this model, accreting matter cools so efficiently that all of the energy released through viscosity can be radiated

⋆ E-mails: amin@shao.ac.cn (AM); abbassi@ipm.ir (SA); n_beiranvand@std.du.ac.ir (NB)

locally. However, there exist distinct branches of steady disc solutions in which this assumption is violated. In a radiatively inefficient accretion flow (hereafter RIAF), the energy released via viscosity is stored as entropy and transported inward with accretion, so the flow becomes very hot and produces high-energy emission (see Kato, Fukue & Mineshige 2008 for a review).

In the case of low mass accretion rate, $\dot{M} \leq 0.1 L_{\rm E}/c^2$, we expect optically thin advection-dominated accretion flows (ADAFs/RIAFs) with insufficient cooling (Ichimaru 1977; Rees et al. 1982; Narayan & Yi 1994, 1995a,b; Abramowicz et al. 1995). ADAFs were adopted to describe the low/hard state of black hole binaries and low-luminosity active galactic nuclei (AGNs), such as the supermassive black hole in the centre of our Galaxy (Sgr A*). If the accretion rate is mildly low, $\dot{M} \leq L_{\rm E}/c^2$, the disc is in the Shakura & Sunyaev standard state (SSD), i.e. it is geometrically thin and optically thick. The SSD model can be applied to the high/soft state of black hole binaries and even luminous AGNs. Moreover, if the mass accretion rate is very high, $\dot{M} \geq L_{\rm E}/c^2$, the disc is categorized as in a supercritical state (slim disc), meaning that the disc is optically and geometrically thick. This bright branch may be applied to the very high state of black hole binaries and super-Eddington sources.

ADAF models have garnered much attention and rapid progress has been made in this field. An extensive discussion of advection-dominated accretion discs was begun by Narayan & Yi (1994, 1995a). They solved the disc structure along the θ direction using a self-similar method in the radial direction. Moreover, several numerical simulations (hydrodynamical and magnetohydrodynamical) have been performed to study the structure of ADAFs (see Stone, Pringle & Begelman 1999; Stone & Pringle 2001; DeVilliers, Hawley & Krolik 2003; Pen, Matzener & Wong 2003; Okuda et al. 2005; Yuan & Bu 2010; Mckinney, Tchekhovskoy & Blandford 2012; Yuan et al. 2012a,b). These models have been used to interpret the spectra of black hole X-ray binaries in their quiescent or low/hard state as an alternative to the Shapiro, Lightman & Eardley (1976, hereafter SLE) solutions. Since ADAFs have large radial velocities, accreting matter carries thermal energy into the black hole. Thus, advective energy transport will act against thermal instability. For this reason, ADAFs have been widely used to explain observations of galactic black hole candidates (e.g. Narayan, Maclintock & Yi 1996; Hameury et al. 1997), the spectral transition of Cyg X-1 (Esin et al. 1996) and the multi-wavelength spectral properties of Sgr A* (Narayan & Yi 1995b; Manmoto et al. 2000; Narayan, Kato & Honma 1997; Yuan, Quataert & Narayan 2003, 2004).

Many ADAF-like models have been proposed, including outflows, convection, etc. In this regard, the luminous hot accretion flow (LHAF) model by Yuan (2001) is a development of ADAF to higher accretion rates. Moreover, the convection-dominated accretion flow (CDAF) model (Narayan, Igumenshchev & Abramowicz 2000; Quataert & Gruzinov 2000) proposes that accretion flows are convectively unstable. In addition, the adiabatic inflow–outflow solution (ADIOS) model is an additional development that was suggested by Blandford & Begelman (1999, 2004). Recently, however, the simulations of Yuan et al. (2012b) have shown that the convection model is not a complete model by which to explain outflows.

It has been observationally verified that some of the angular momentum in an accretion disc is dissipated outwards by outflows in the form of wind or jets from such systems (Whelan et al. 2005; Bally, Reipurth & Davis 2007; Dionatos et al. 2009, 2010). These outflows, which characteristically cause the loss of angular momentum, mass and thermal energy, are classified as winds or jets based on their collimation. However, this classification is not exactly clear because some observed systems contain both types of outflow (e.g. Piran 1977; Blandford & Payne 1982; Pudritz 1985). These kinds of outflows are seen in all sorts of objects, from microquasars and young stellar objects (YSOs) to AGNs, etc., which is a good indication of the range of scales involved in these phenomena. The cause of these outflows is the accretion mechanism itself, so it is imperative to understand this mechanism, particularly at earlier stages when most of the matter is accreted by a central object.

It is found that the rate of mass loss is proportional to the disc size and the mass of the central object, possibly through a power-law dependence (Abbassi, Nourbakhsh & Shadmehri 2013). From the first star formation models, which considered an accretion flow without wind, it was found that mass accretion is constant at $\sim 2 \times 10^{-6}\,{\rm M}_\odot\,{\rm yr}^{-1}$, as the collapse proceeds from inside out at the local sound speed. However, as a result of outflows the accretion rate varies with radius as a power law, with a power-law index of the order of unity (see e.g. Blandford & Begelman 1999; Abbassi, Ghanbari & Ghasemnezhad 2010; Yuan et al. 2012a,b; Abbassi et al. 2013). In the earlier phases of star formation, the accretion rate is very high ($\sim 10^6\,{\rm M}_\odot\,{\rm yr}^{-1}$) and the mass loss in the system is in the form of winds, with the mass-loss rate being $\sim 0.1\dot{M}$ (Gorti & Hollenbach 2009). What exactly drives these winds is still not very clear. The emission mechanism of disc winds relies on a variety of physical phenomena, such as the effects of magnetic fields, electric fields generated by the relative separation between ions and electrons, electron–positron pair production and their coupling with the radiation field in disc winds, etc. (Takahara, Rosner & Kusunose 1989).

ADAF solutions predict a high temperature for accretion material. Consequently, the gas is ionized and will be affected by a magnetic field. Magnetic fields therefore play an important role in the dynamics of accretion flows and probably in the creation of outflows, winds or jets. Kaburaki (2000), Shadmehri & Khajenabi (2005), Abbassi, Ghanbari & Salehi (2006), Ghanbari, Salehi & Abbassi (2007), Abbassi, Ghanbari & Najjar (2008), Xie & Yuan (2008), Abbassi et al. (2010) and Bu, Yuan & Xie (2009) have tried to solve the magnetohydrodynamics (MDH) equations of magnetized ADAFs analytically. They showed that the presence of a magnetic field and its associated resistivity can change the picture considerably with regard to accretion flows.

As was mentioned, Narayan & Yi used the self-similar method in the radial direction and solved the disc structure along the θ direction. The self-similar approach adopted by Narayan & Yi (1995b) is only partially supported by numerical simulations, i.e. there exists a new class of accretion flows that are hot, optically thin and advection-dominated. On the other hand, a shortcoming is also obvious, i.e. the lack of an outflow. Thus, it is not consistent with the new developments in hot accretion flow theory. Also, recent theoretical work (Blandford & Begelman 1999) and numerical simulations (Stone, Pringle & Begelman 1999; Stone & Pringle 2001; De Villiers et al. 2005; Ohsuga & Mineshige 2011; Yuan et al. 2012a,b) indicate that outflows are commonly observed to be associated with hot accretion flows. More importantly, there is compelling observational evidence for the existence of outflows in hot accretion systems, e.g. our Galactic Centre and NGC 3115 (see Xie & Yuan 2012, for a short summary). Moreover, numerical simulations indicate that v_θ is non-zero (see Stone, Pringle & Begelman 1999; Ohsuga & Mineshige 2011; Yuan et al. 2012b). Besides, numerical calculations indicate that it is very difficult to find an outflow solution with $v_\theta = 0$ (Narayan & Yi 1995), whereas with non-zero v_θ an outflow can be found (e.g. Xue & Wang 2005) and v_r will be positive.

Recently, Jiao & Wu (2011) solved a set of hydrodynamical equations for accretion discs in spherical coordinates (r, θ, φ) and obtained the explicit structure along the θ direction. They assumed $v_\theta \neq 0$ and used a self-similar treatment that leads to an accretion outflow solution for ADAFs. ADAF solutions with wind were reported previously by Abbassi et al. (2008, 2010) and Mosallanezhad, Khajavi & Abbassi (2013), where the effects of wind and outflow are achieved by adding the relevant terms in the MHD equations. It means that an outflow will appear through a power-law assumption in the MHD equations. The solutions of Jiao & Wu (2011) show that when we assume $v_\theta \neq 0$ by adopting a proper boundary-condition self-similar solution, it will lead to constant inflow–outflow behaviour. In this article we will try to develop the solutions of Jiao & Wu (2011) by adding a toroidal magnetic field and its corresponding resistivity using the self-similar method. Recent numerical simulations support the idea that the mass accretion rate, radial velocity and density can be well approximated as power laws (see e.g. Stone, Pringle & Begelman 1999; Yuan et al. 2012b). All of these power-law profiles are consistent with the self-similar methodology adopted in our work. Although the existence of a self-similar solution in no way guarantees that this solution is relevant to real accretion flows (particularly near to boundaries), it is nevertheless likely to provide a good indication of how realistic flows will behave.

The structure of this article is as follows. In Section 2, we describe basic equations and give a self-similar solution in the radial direction corresponding to an ADAF model. Boundary conditions are presented in Section 3. In Section 4, we show numerical results and discuss the variation and physical meaning of each parameter, from the equatorial plane to the surface of the disc. Conclusions are presented in Section 5.

2 BASIC EQUATIONS AND SELF-SIMILAR SOLUTIONS

2.1 Basic equations

In this section we derive the basic equations of optically thin advection-dominated accretion flows under the magnetohydrodynamics approximation and in a non-relativistic regime. We neglect the effect of self-gravity in our model. The magnetic field is considered with toroidal configurations and, in addition to relativistic effects being ignored, we have used Newtonian gravity. The disc is supposed to be turbulent and possesses an effective turbulent viscosity. The α-prescription for viscosity was adopted. We have assumed that the energy generated due to viscosity and magnetic resistivity is balanced by a combination of radiative and advective cooling. Thus, resistive MHD equations are involved in the form of the continuity equation, equation of motion, energy equation and induction equation, which can be respectively written as follows:

$$\frac{\mathrm{d}\rho}{\mathrm{d}t} + \rho\nabla\cdot\boldsymbol{v} = 0, \tag{1}$$

$$\rho\frac{\mathrm{d}\boldsymbol{v}}{\mathrm{d}t} = -\rho\nabla\psi - \nabla p + \frac{1}{c}\boldsymbol{J}\times\boldsymbol{B} + \nabla\cdot\boldsymbol{T}, \tag{2}$$

$$\rho\left[\frac{\mathrm{d}e}{\mathrm{d}t} + p\frac{\mathrm{d}}{\mathrm{d}t}\left(\frac{1}{\rho}\right)\right] = Q_+ - Q_- \equiv Q_{\rm adv}, \tag{3}$$

$$\frac{\partial\boldsymbol{B}}{\partial t} = \nabla\times\left(\boldsymbol{v}\times\boldsymbol{B} - \frac{4\pi}{c}\eta\boldsymbol{J}\right). \tag{4}$$

In the above MHD equations, ρ, $\boldsymbol{v}\equiv(v_r, v_\theta, v_\varphi)$, ψ, p, $\boldsymbol{B}$, $\boldsymbol{J}\equiv(c/4\pi)\nabla\times\boldsymbol{B}$ and $\boldsymbol{T}$ are the mass density, velocity vector, gravitational potential, pressure, magnetic field, current density and the tensor of viscous stress, respectively. Here, $\mathrm{d}/\mathrm{d}t = \partial/\partial t + \boldsymbol{v}\cdot\nabla$. We adopt spherical coordinates (r, θ, φ) to solve these equations. We consider a Newtonian potential $\psi = GM_*/r$, where G is the gravitational constant, M_* is the central object mass and r is the spherical radial coordinate. In our calculation, we use only the $r\varphi$-component of the viscous stress tensor, which is $t_{r\varphi} = \nu\rho\partial(v_\varphi/r)/\partial r$, where ν is the kinematic viscosity coefficient and will be defined later. In the energy equation, e is the internal energy and can be expressed as

$$e = \frac{p}{\rho(\gamma-1)}, \tag{5}$$

where γ is the ratio of specific heats and is considered as a constant input parameter. On the right-hand side of the energy equation we have

$$Q_+ - Q_- \equiv Q_{\rm adv}; \tag{6}$$

here, $Q_{\rm adv}$ is the advection transfer of energy, Q_- shows the energy loss through radiative cooling and Q_+ represents the dissipation rate of heating due to viscosity and resistivity, $Q_+ = Q_{\rm vis} + Q_B$, which can be defined as

$$Q_{\rm vis} = t_{r\varphi}r\frac{\partial}{\partial r}\left(\frac{v_\varphi}{r}\right) = \nu\rho r^2\left[\frac{\partial}{\partial r}\left(\frac{v_\varphi}{r}\right)\right]^2, \tag{7}$$

$$Q_B = \frac{\eta}{4\pi}\left|\nabla\times\boldsymbol{B}\right|^2, \tag{8}$$

where η is the magnetic diffusivity parameter and Q_B is the hitting rate due to the resistance of fluid against the motion of charges. In other words, Q_B is the Joule hitting or resistivity hitting, which is equal to $J\cdot E$, where E is the electric field in the comoving frame. We consider that ν and η have the same units and for both of them we use the general case:

$$\nu = \alpha\frac{p_{\rm gas}^{\mu}}{\rho\Omega_k}\left(p_{\rm gas}+p_{\rm mag}\right)^{1-\mu} \equiv \alpha\frac{p}{\rho\Omega_k}\left(1+\frac{B^2}{8\pi p}\right)^{1-\mu}, \tag{9}$$

$$\eta = \eta_0\frac{p_{\rm gas}^{\mu}}{\rho\Omega_k}\left(p_{\rm gas}+p_{\rm mag}\right)^{1-\mu} \equiv \eta_0\frac{p}{\rho\Omega_k}\left(1+\frac{B^2}{8\pi p}\right)^{1-\mu}; \tag{10}$$

here, $p_{\rm mag}(=B^2/8\pi)$ is the magnetic pressure, $\Omega_k = \sqrt{GM_*/r^3}$ is the Keplerian angular speed and also α, η_0 and μ are positive constants less than 1. Thus, the right-hand side of the energy equation will be

$$Q_{\rm adv} \equiv Q_+ - Q_- = Q_+\left(1-\frac{Q_-}{Q_+}\right) = fQ_+ \tag{11}$$

and

$$Q_+ = \nu\rho r^2\left[\frac{\partial}{\partial r}\left(\frac{v_\varphi}{r}\right)\right]^2 + \frac{\eta}{4\pi}\left|\nabla\times\boldsymbol{B}\right|^2, \tag{12}$$

where f is the advection parameter defined by Narayan & Yi (1994). Although this parameter varies with radius r and depends on the heating and cooling processes, we consider it as a constant here. We fix $\mu = 0$ throughout this article. For simplicity, the flow is assumed to be steady and axisymmetic ($\partial/\partial t = \partial/\partial\varphi = 0$). We also consider the toroidal component of magnetic field, $\boldsymbol{B} = (0, 0, B_\varphi)$. Most simulations in accretion discs show that the toroidal component of magnetic field is enhanced due to the rotating disc. We can say that

utilizing the toroidal component is the right choice as regards the physics of accretion processes. Now we can reformulate the basic equations (1)–(4) in spherical coordinates as

$$\frac{1}{r^2}\frac{\partial}{\partial r}(r^2\rho v_r)+\frac{1}{r\sin\theta}\frac{\partial}{\partial\theta}(\sin\theta\rho v_\theta)=0, \tag{13}$$

$$\rho\left[v_r\frac{\partial v_r}{\partial r}+\frac{v_\theta}{r}\left(\frac{\partial v_r}{\partial\theta}-v_\theta\right)-\frac{v_\varphi^2}{r}\right]=-\rho\frac{GM_*}{r^2}-\frac{\partial p}{\partial r}-\frac{B_\varphi}{4\pi r}\frac{\partial}{\partial r}(rB_\varphi), \tag{14}$$

$$\rho\left[v_r\frac{\partial v_\theta}{\partial r}+\frac{v_\theta}{r}\left(\frac{\partial v_\theta}{\partial\theta}+v_r\right)-\frac{v_\varphi^2}{r}\cot\theta\right]=-\frac{1}{r}\frac{\partial p}{\partial\theta}-\frac{1}{4\pi}\frac{B_\varphi}{r\sin\theta}\frac{\partial}{\partial\theta}(B_\varphi\sin\theta), \tag{15}$$

$$\rho\left[v_r\frac{\partial v_\varphi}{\partial r}+\frac{v_\theta}{r}\frac{\partial v_\varphi}{\partial\theta}+\frac{v_\varphi}{r}(v_r+v_\theta\cot\theta)\right]=\frac{1}{r^3}\frac{\partial}{\partial r}\left(\nu\rho r^4\frac{\partial}{\partial r}\left(\frac{v_\varphi}{r}\right)\right), \tag{16}$$

$$\frac{\rho}{\gamma-1}\left[v_r\frac{\partial}{\partial r}\left(\frac{p}{\rho}\right)+\frac{v_\theta}{r}\frac{\partial}{\partial\theta}\left(\frac{p}{\rho}\right)\right]-\frac{p}{\rho}\left(v_r\frac{\partial\rho}{\partial r}+\frac{v_\theta}{r}\frac{\partial\rho}{\partial\theta}\right)=f\frac{p}{\rho\Omega_k}\left(1+\frac{B^2}{8\pi p}\right)\left\{\alpha\rho r^2\left(\frac{\partial}{\partial r}\left(\frac{v_\varphi}{r}\right)\right)^2+\frac{\eta_0}{4\pi}|\nabla\times\boldsymbol{B}|^2\right\}, \tag{17}$$

$$\frac{\partial}{\partial r}(rv_rB_\varphi)+\frac{\partial}{\partial\theta}(v_\theta B_\varphi)-\frac{\partial}{\partial r}\left[\eta_0\frac{p}{\rho\Omega_k}\left(1+\frac{B^2}{8\pi p}\right)\frac{\partial}{\partial r}(rB_\varphi)\right]-\frac{\partial}{\partial\theta}\left[\frac{p}{\rho\Omega_k}\left(1+\frac{B^2}{8\pi p}\right)\frac{\eta_0}{r\sin\theta}\frac{\partial}{\partial\theta}(B_\varphi\sin\theta)\right]=0. \tag{18}$$

2.2 Self-similar solutions

The basic equations of the model are a set of partial differential equations, which have a very complicated structure. In fact, these partial differential equations are converted into ordinary differential equations by using the assumption of radial self-similarity, although investigation is required as to whether there are any critical points or not. The self-similar method is one of the most useful and powerful techniques for solving differential equations. By this method, we can solve a set of coupled differential equations analytically or semi-analytically. The disc equations reduce from partial to ordinary differential equations under the assumption of radial self-similarity, which implies that all quantities are described by power laws in spherical radius r for a fixed inclination angle. This assumption is widely used in the literature of black hole accretion discs (see Narayan & Yi 1994, 1995; Akizuki & Fukue 2006; Kato et al. 2008). The self-similar scaling for density and velocities shows very good agreement with recent numerical simulations of accretion discs (Stone, Pringle & Begelman 1999; De Villiers et al. 2005; Beckwith, Hawley & Krolik 2009; Yuan et al. 2012a,b).

Generally, self-similar solutions are divided into two chief categories: temporal self-similar answers and spatial self-similar answers. Because the equations of the system depend on time, we can search for answers that describe the temporal change of physical quantities in such a way that the change of each quantity at any instant of time is similar to the change in the others. However, the second category, spatially self-similar solutions, are used in this article. Essentially, spatially self-similar solutions describe the behaviour of physical quantities in such a manner that, at any distance from the centre of the system, the difference from other points is only a constant factor. As a result, these answers are usually power functions of position. We therefore solve a set of equations that depend on (r,θ). Thus our self-similar solutions must be in the form of (r,θ). Physical quantities are assumed to be unknown powers of (r,θ). We then try to put answers in the form of powers in the equations to determine the power in a way that satisfies the equations. If we succeed, it means that the equations have self-similar answers.

We adopt the self-similar assumption in the radial direction to simplify equations (13)–(18) as follows:

$$\rho(r,\theta)=\rho(\theta)r^{-n}, \tag{19}$$

$$v_r(r,\theta)=v_r(\theta)\sqrt{\frac{GM_*}{r}}, \tag{20}$$

$$v_\theta(r,\theta)=v_\theta(\theta)\sqrt{\frac{GM_*}{r}}, \tag{21}$$

$$v_\varphi(r,\theta)=v_\varphi(\theta)\sqrt{\frac{GM_*}{r}}, \tag{22}$$

$$p(r,\theta)=p(\theta)GM_*r^{-n-1}, \tag{23}$$

$$B_\varphi(r,\theta)=b(\theta)\sqrt{GM_*}r^{-(n/2)-(1/2)}. \tag{24}$$

Our set of self-similar solutions is similar to that of Narayan & Yi (1995) and we add a new equation (24) for the toroidal component of magnetic field. We follow Xue & Wang (2005) and Jiao & Wu (2011) in setting $v_\theta\neq0$ and study the structure of discs with the presence of outflows. With self-similar solutions (19)–(24), equations (13)–(18) are reduced to a set of differential equations as follows:

$$\rho(\theta)\left[\left(n-\frac{3}{2}\right)v_r(\theta)-v_\theta(\theta)\cot\theta-\frac{\mathrm{d}v_\theta(\theta)}{\mathrm{d}\theta}\right]-v_\theta\frac{\mathrm{d}\rho(\theta)}{\mathrm{d}\theta}=0, \tag{25}$$

$$\rho(\theta)\left[\frac{1}{2}v_r^2(\theta)+v_\theta(\theta)^2+v_\varphi^2(\theta)-v_\theta(\theta)\frac{\mathrm{d}v_r(\theta)}{\mathrm{d}\theta}-1\right]+(n+1)p(\theta)+\frac{1}{8\pi}(n-1)b^2(\theta)=0, \tag{26}$$

$$\rho(\theta)\left[v_\varphi^2(\theta)\cot\theta-\frac{1}{2}v_r(\theta)v_\theta(\theta)-v_\theta(\theta)\frac{\mathrm{d}v_\theta(\theta)}{\mathrm{d}\theta}\right]-\frac{\mathrm{d}p(\theta)}{\mathrm{d}\theta}-\frac{1}{4\pi}b(\theta)\left\{b(\theta)\cot\theta+\frac{\mathrm{d}b(\theta)}{\mathrm{d}\theta}\right\}=0, \tag{27}$$

$$v_\varphi(\theta)\left[\frac{3}{2}\alpha(n-2)p(\theta)\left(1+\frac{b^2(\theta)}{8\pi p(\theta)}\right)-\rho(\theta)\left\{v_\theta(\theta)\cot\theta+\frac{1}{2}v_r(\theta)\right\}\right]-\rho(\theta)v_\theta(\theta)\frac{\mathrm{d}v_\varphi(\theta)}{\mathrm{d}\theta}=0, \tag{28}$$

$$p(\theta)\Bigg\{\gamma v_\theta(\theta)\frac{\mathrm{d}\rho(\theta)}{\mathrm{d}\theta}-(n\gamma-n-1)v_r(\theta)\rho(\theta)+f(\gamma-1)\times\left(1+\frac{b^2(\theta)}{8\pi p(\theta)}\right)\Bigg[\frac{9}{4}\alpha\rho(\theta)v_\varphi^2(\theta)\frac{\eta_0}{4\pi}\Bigg\{\left(b(\theta)\cot\theta+\frac{\mathrm{d}b(\theta)}{\mathrm{d}\theta}\right)^2+\left(\frac{1}{2}(n-1)b(\theta)\right)^2\Bigg\}\Bigg]\Bigg\}-\rho(\theta)v_\theta(\theta)\frac{\mathrm{d}p(\theta)}{\mathrm{d}\theta}=0, \tag{29}$$

$$\eta_0\frac{p(\theta)}{\rho(\theta)}\Bigg\{\left(1+\frac{b^2(\theta)}{8\pi p(\theta)}\right)\Bigg\{\frac{\mathrm{d}^2b(\theta)}{\mathrm{d}\theta^2}+\frac{\mathrm{d}b(\theta)}{\mathrm{d}\theta}\cot\theta+\frac{1}{4}n(n-1)b(\theta)-\frac{b(\theta)}{\sin\theta^2}\Bigg\}+\left(b(\theta)\cot(\theta)+\frac{\mathrm{d}b(\theta)}{\mathrm{d}\theta}\right)\times\Bigg[\left(1+\frac{b^2(\theta)}{8\pi p(\theta)}\right)\Bigg\{\frac{1}{p(\theta)}\frac{\mathrm{d}p(\theta)}{\mathrm{d}\theta}-\frac{1}{\rho(\theta)}\frac{\mathrm{d}\rho(\theta)}{\mathrm{d}\theta}\Bigg\}+\frac{b^2(\theta)}{8\pi p(\theta)}\Bigg\{2\frac{1}{b(\theta)}\frac{\mathrm{d}b(\theta)}{\mathrm{d}\theta}-\frac{1}{p(\theta)}\frac{\mathrm{d}p(\theta)}{\mathrm{d}\theta}\Bigg\}\Bigg]\Bigg\}+\frac{n}{2}v_r(\theta)b(\theta)-v_\theta(\theta)\frac{\mathrm{d}b(\theta)}{\mathrm{d}\theta}-b(\theta)\frac{\mathrm{d}v_\theta(\theta)}{\mathrm{d}\theta}=0, \tag{30}$$

with six dimensionless functions $v_r(\theta)$, $v_\theta(\theta)$, $v_\varphi(\theta)$, $\rho(\theta)$, $p(\theta)$ and $b(\theta)$. This system can be solved with our boundary conditions as expressed in the next section.

3 BOUNDARY CONDITIONS

As we mentioned, our equation reduces to a set of six ODEs, with six dimensionless functions $v_r(\theta)$, $v_\theta(\theta)$, $v_\varphi(\theta)$, $\rho(\theta)$, $p(\theta)$ and $b(\theta)$, the variable θ and six input parameters (α, f, γ, n, η_0, β_0), where β_0 is the ratio of the gas pressure to the magnetic pressure at the equatorial plane:

$$\beta_0=\left.\frac{p_{\rm gas}}{p_{\rm mag}}\right|_{90^\circ}=\left.8\pi\frac{p}{b^2}\right|_{90^\circ}, \tag{31}$$

which is considered to be constant. This set of ODEs can be solved numerically with proper boundary conditions. We assume the structure of the disc is symmetric to the equatorial plane, and thus we have

$$\theta=90^\circ:\qquad v_\theta=\frac{\mathrm{d}\rho}{\mathrm{d}\theta}=\frac{\mathrm{d}p}{\mathrm{d}\theta}=\frac{\mathrm{d}v_r}{\mathrm{d}\theta}=\frac{\mathrm{d}v_\varphi}{\mathrm{d}\theta}=\frac{\mathrm{d}b}{\mathrm{d}\theta}=0. \tag{32}$$

It is obvious that only five conditions are independent and then we require other boundary conditions. As far as we know, the mass density declines at the equatorial plane to the vertical axis. As the next condition we optimize the maximum density to unity, $\rho(90^\circ)=1$. Now, if we put the above boundary conditions into equations (25)–(30), we obtain

$$\left.\frac{\mathrm{d}v_\theta}{\mathrm{d}\theta}\right|_{90^\circ}=\left(n-\frac{3}{2}\right)v_r\,|_{90^\circ}, \tag{33}$$

$$\frac{1}{2}\left.v_r^2\right|_{90^\circ}+\left.v_\varphi^2\right|_{90^\circ}+\left[(n+1)+\frac{(n-1)}{\beta_0}\right]p\,|_{90^\circ}-1=0, \tag{34}$$

$$v_r\,|_{90^\circ}=E_1p\,|_{90^\circ}, \tag{35}$$

$$\left.v_\varphi^2\right|_{90^\circ}=\frac{E_1E_3-E_4}{E_2}p\,|_{90^\circ}, \tag{36}$$

$$\left.\frac{\mathrm{d}b^2}{\mathrm{d}\theta^2}\right|_{90^\circ}=\left(E_1E_5+E_6\right)\left.\frac{b}{p}\right|_{90^\circ}, \tag{37}$$

where

$$E_1=3\alpha(n-2)\left(1+\beta_0^{-1}\right), \tag{38}$$

$$E_2=\frac{9}{4}f\alpha(\gamma-1)\left(1+\beta_0^{-1}\right), \tag{39}$$

$$E_3=n\gamma-n-1, \tag{40}$$

$$E_4=\frac{1}{2}f\eta_0(\gamma-1)\beta_0^{-1}(n-1)^2\left(1+\beta_0^{-1}\right), \tag{41}$$

$$E_5=-\frac{n}{2\eta_0}\left(1+\beta_0^{-1}\right), \tag{42}$$

$$E_6=1-\frac{1}{4}n(n-1). \tag{43}$$

By substituting equations (35) and (36) into equation (34), the gas pressure in the equatorial plane will be

$$p\,|_{90^\circ}=\frac{-B\pm\sqrt{B^2-4AC}}{2A}. \tag{44}$$

Here,

$$A=\frac{E_1^2}{2}, \tag{45}$$

$$B=\frac{E_1E_3-E_4}{E_2}+(n+1)+(n-1)\beta_0^{-1}, \tag{46}$$

$$C=-1. \tag{47}$$

Having already defined the relation between gas pressure and alternative quantities, we have the value of all quantities in the equatorial plane, $\theta=90^\circ$. We know the solution with $n=3/2$ examined by Narayan & Yi (1995a,b). Then, following the work done by Jiao & Wu (2011), we consider $n\leq3/2$. In this way, it is seen from equations (38)–(43) that E_1, E_5 parameters have negative values ($E_1<0$, $E_5<0$), while E_6 is positive in this regime of density index. Therefore it is obvious that the right-hand side of equation (37) will be positive. This indicates that at mid-plane we have $\mathrm{d}^2b/\mathrm{d}\theta^2>0$. This very interesting mathematical result shows that magnetic pressure has a minimum value at the equatorial plane. Due to this, the ratio of gas pressure to the magnetic pressure, $\beta(\theta)$, will have a maximum in the mid-plane of the disc. We will consider $10^2\leq\beta_0\leq10^4$ in our figures. The upper boundary condition is adjacent to the vertical axis, $\theta=0^\circ$, where the gas pressure and mass density become almost zero (defining the upper limit as $\theta_{\rm b}$). Also, there must be a θ_0 at a particular point where the radial velocity is equal to zero, $v_r(\theta_0)=0$, and after this bending point the inflow material is deflected to the outflow. Hence we can define the inflow region as the region where the inflow of matter is directed towards the central mass and has a negative value, $\theta_0<\theta<90^\circ$, and the

outflow region as the region where radial velocity has a positive value, $\theta_b < \theta < \theta_0$. According to Xue & Wang (2005) and Jiao & Wu (2011), the mass inflow and outflow rates can be written as

$$\dot{M}(r) = \dot{M}_{\rm inflow}(r) + \dot{M}_{\rm outflow}(r) = 4\pi\sqrt{GM_*}r^{(3/2)-n} \times \left[\int_{\theta_b}^{\theta_0} \rho(\theta)v_r(\theta)\sin\,{\rm d}\theta + \int_{\theta_0}^{\pi/2} \rho(\theta)v_r(\theta)\sin\,{\rm d}\theta\right]. \quad (48)$$

Based on the above equation, mass density is function of r and only when $n = -3/2$ does the mass density become independent of radius. Also, if the outflow rate equals the inflow rate of material at a certain radius, the second law of thermodynamics is violated (see Xue & Wang 2005 and Jiao & Wu 2011 for more details).

4 NUMERICAL RESULTS

In this section, we will investigate the role of magnetic field parameters β_0, η_0 and also n, α and γ parameters on the vertical structure of accretion discs and basic dynamical quantities of our model. As previously mentioned, we have a positive value for the radial velocity of accretion material, $v_r(\theta)$. In fact, this positive value indicates that the fluid is moving away from the central massive accretor; this phenomenon will escalate with the decrease of θ and also move towards the surface of the accretion disc. Indeed, due to the very low density around the vertical axis, $\theta = 0$, numerical errors will appear and we have to finish our calculation at this angle. Therefore, this point is considered as the surface of the accretion disc. In other words, as is expressed in previous works (Jiao & Wu 2011), according to the sign of the radial velocity, three different regions are distinguished in an accretion disc. One is the predominant region, which is called the inflow region and starts from mid-plane and continues to where the radial velocity equals zero ($v_r(\theta_0) = 0$). Here θ_0 indicates the angle at which the radial velocity is zero. Actually, in the interval $\theta_0 \leq \theta \leq 90^\circ$, the accretion flow moves towards the massive accretor. For this reason it is called the inflow region and it is obvious that the accretion rate will be negative there. The next area that has been located just after the inflow region and continues to the surface of the disc is called the outflow region. In this area, the value of the radial velocity is positive, meaning that the accretion flow is moving away from the central accretor. This region is not very wide and, as is anticipated by calculation of the mass accretion rate in this area, this rate is less than unity; this does not violate the second law of thermodynamics. Also, a large fraction of accretion flow at a certain radius inclines towards the massive accretor and does not escape from the disc by wind or outflow (see Xue & Wang 2005; Jiao & Wu 2011 for more details). Finally, the third region is called the wind region: a very narrow area located between the surface of the disc and the vertical axis; we do not have much information about this area owing to some drawbacks in the self-similar solution.

Fig. 1 shows the role of magnetic field parameters β_0 and η_0, viscosity parameter α and density index n on the radial velocity of the accretion flow along the θ direction. Other fixed parameters are mentioned at the top of each panel. In the top left panel, the radial velocity along the θ direction is seen for different values of β_0. Here β_0 demonstrates the ratio of gas to magnetic pressure in the equatorial plane. According to Fig. 1, β_0 does not have any effect on the inflow region and only changes the outflow value. It is seen that if the magnetic pressure is increased, the area of the outflow region is decreased (the small value of β_0 shows a high value for magnetic pressure). This implies that the toroidal

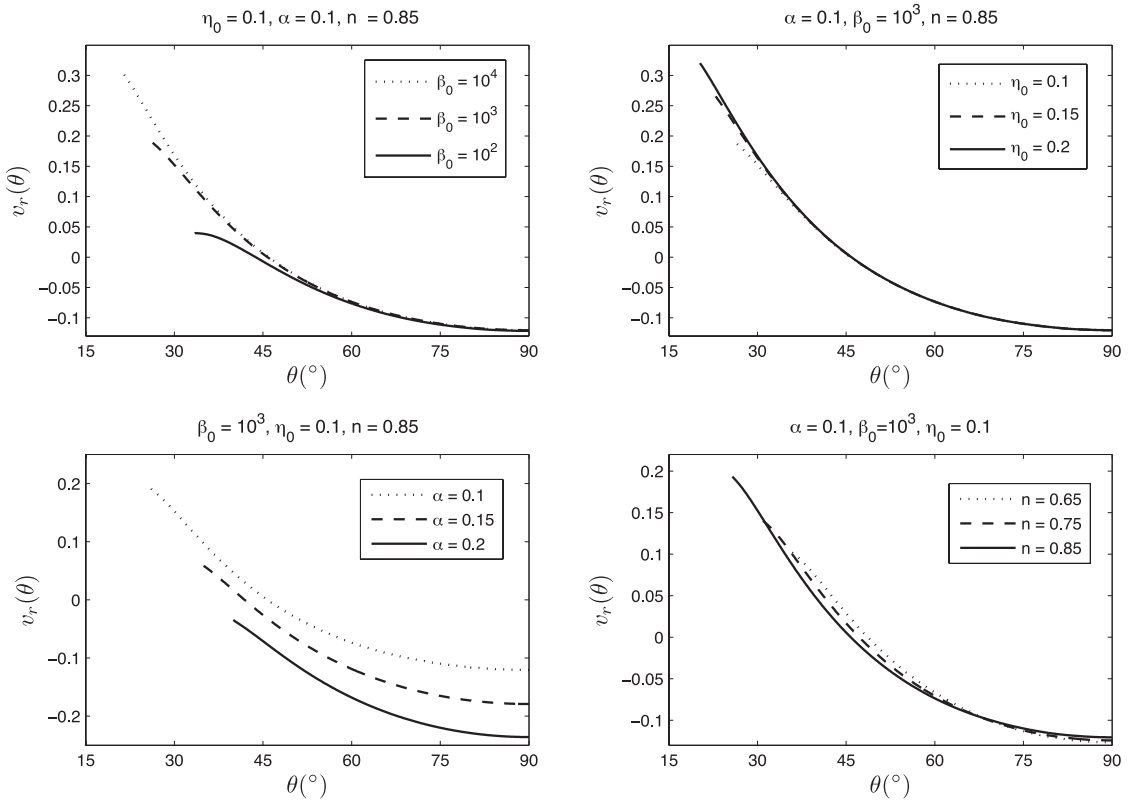

Figure 1. Radial flow speed $v_r(\theta)$ along the θ direction, corresponding to different input parameters β_0, η_0, α and n. Here $\gamma = 5/3$ and $f = 1$.

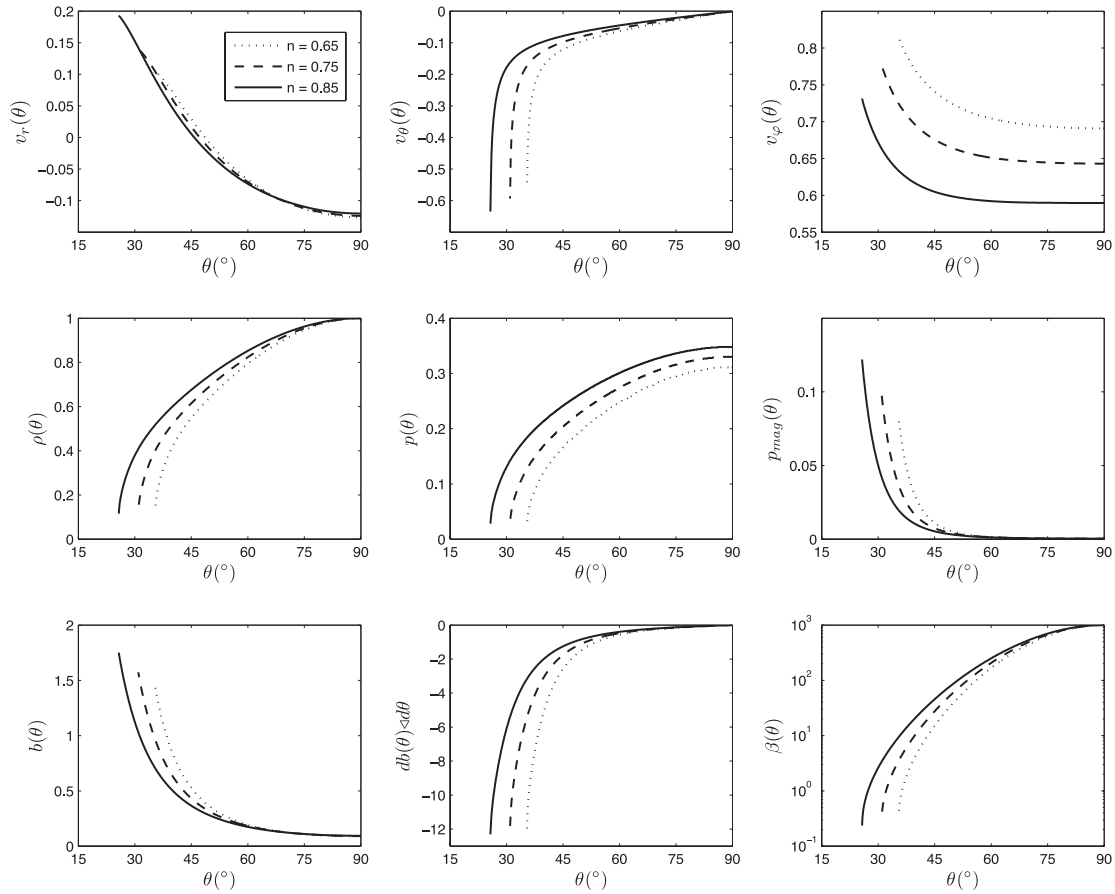

Figure 2. Profiles of the physical variables corresponding to the ADAF model along the θ direction for different values of density index n. The dotted, dashed and solid lines denote $n = 0.65, 0.75$ and 0.85 respectively. Here $\beta_0 = 10^3$, $\alpha = 0.1$, $\gamma = 5/3$, $f = 1$ and $\eta_0 = 0.1$.

component of the magnetic field prevents material from leaving the surface of the disc. In addition, it is clear from this panel that the thickness of the disc decreases with increasing magnetic field in the equatorial plane. The top right panel of this figure shows the role of different values of η_0 on radial velocity along the θ direction. As shown in this panel, unlike the ratio of gas to magnetic pressure in mid-plane, the magnetic diffusivity parameter, η_0, increases in the outflow region. Actually, the radial velocity will be more positive in this region, but there are no special effects on the thickness and inflow region. The bottom left panel contains different values of the viscosity parameter, α. We assume this quantity to be in range $0 < \alpha \leq 0.2$, according to observations. According to this panel, the inflow area increases with increasing α but the thickness of the disc and outflow region decrease. Additionally, for $\alpha > 0.2$ the value of $v_r(\theta)$ is negative. Finally, the bottom right panel is plotted for different values of the density index, n. The anticipated value of n is smaller than unity (Yuan et al. 2012a,b). This panel shows an increase in the outflow region and thickness on increasing the density parameter, which is in full agreement with previous studies (Xue & Wang 2005; Jiao & Wu 2011). We have improved the results of previous works by considering the toroidal component of magnetic field. Therefore, these results are much closer to reality.

In Fig. 2, we have studied the effect of the mass-density power-law index, n, on all physical variables of our system. As before, we neglect time dependence and, since we use a self-similar solution along the radial direction, all of the quantities depend on θ only. As a result, we study the variation of quantities as a function of angle. The first row of Fig. 2 includes components of the velocity vector. In these panels, we considered $n = 0.65$, 0.75 and 0.85, shown by dotted, dashed and solid lines respectively. We can see that the radial velocity increases as the density index is enhanced, but other components of the velocity vector $v_\theta(\theta)$ and $v_\varphi(\theta)$ decrease. According to our symmetry, the value of $v_\theta(\theta)$ on the equatorial plane is zero, i.e. $v_\theta(90^\circ) = 0$. Also, the variation of the second component of the velocity vector is non-zero, $\mathrm{d}v_\theta(90^\circ)/\mathrm{d}\theta \neq 0$. As a result of this symmetry, the fluid is directed to the central object in mid-plane and then, by moving towards the vertical axis, we can see that the direction of material becomes inverse and is inclined towards the surface of the disc. This is because the radial velocity of the accretion flow is positive, something that has been considered in previous works (Xue & Wang 2005; Jiao & Wu 2011). An important issue is the sub-Keplerian velocity. In fact, all three components of velocity at all angles have values smaller than Keplerian. The second row of Fig. 2 shows the variation of mass density, gas pressure and magnetic pressure of the fluid with different values of density parameter, n. Since the starting point is on the equatorial of the disc and the maximum value of density belongs to this point, by gradual motion of the surface of the disc we can show a decrease in density that appears in each of the three parameters of n. Also, similarly, the gas pressure will decrease as θ declines. This interesting and new behaviour is related to magnetic pressure variations based on θ. As shown in this panel, magnetic pressure increases as the angle decreases by motion towards the surface of the disc. Actually, by taking this symmetry assumption on the equatorial plane of the disc

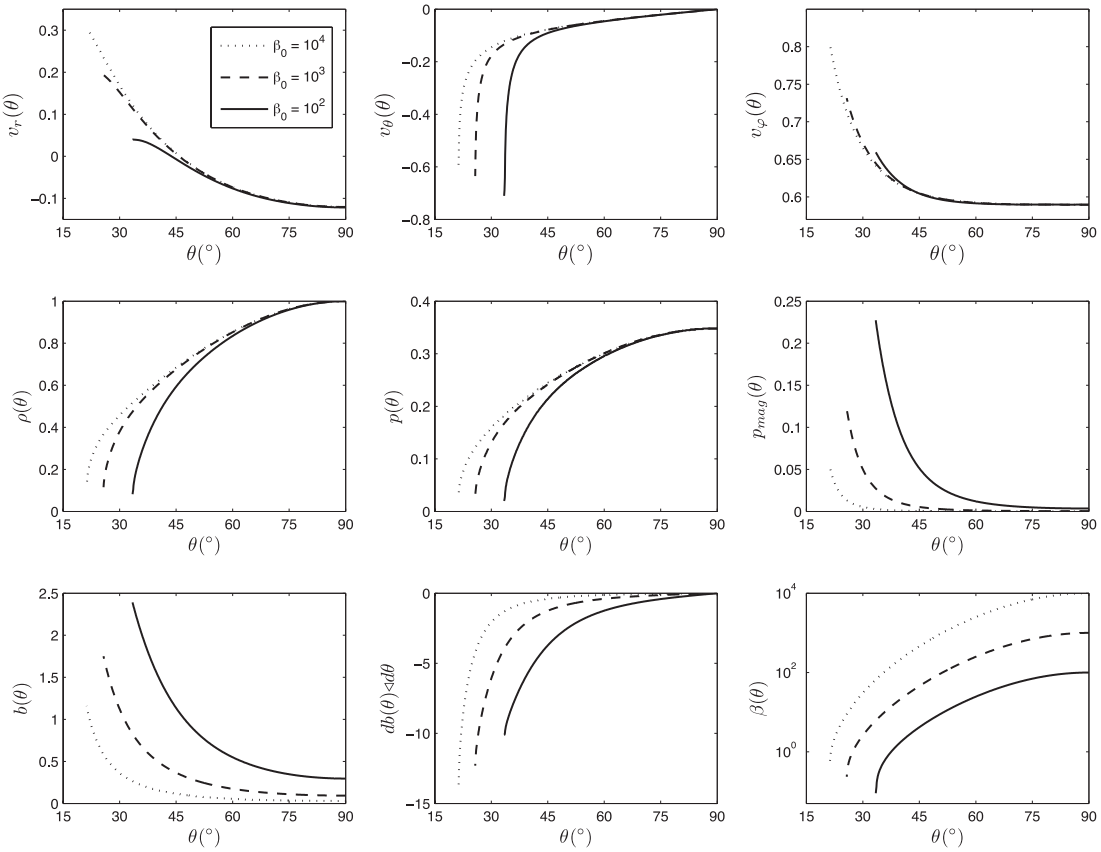

Figure 3. Profiles of the physical variables corresponding to the ADAF model along the θ direction for different values of the ratio of gas pressure to magnetic pressure in the mid-plane of the disc, β_0. The dotted, dashed and solid lines denote $\beta_0 = 10^4$, 10^3 and 10^2 respectively. Here $\alpha = 0.1, \gamma = 5/3, f = 1, \eta_0 = 0.1$ and $n = 0.85$.

and a positive sign for the second derivation of magnetic field at this point, $dB_\varphi(\theta)/d\theta$, due to the fact that the minimum value for magnetic field is in the equatorial plane, we see that an increase of field as θ falls is not far from reality. As a result, the magnetic field on the disc surface is an important parameter for determining the behaviour and structure of the disc. Additionally, as shown in these panels, this parameter leads to an increase in thickness. The last row of Fig. 2 is related to the magnetic field quantities and also the ratio of gas pressure to magnetic pressure, $\beta(\theta)$. It shows that $b(\theta)$ (the toroidal field parameter) increases but derivatives of magnetic field $dB_\varphi(\theta)/d\theta$ and $\beta(\theta)$ decrease as θ decreases. According to Jiao & Wu (2011), if the radial components of the pressure gradient, gravity force, magnetic force and centrifugal force are caused by increasing or decreasing radial velocity, according to the terms in equation (26), and also if we assume a value of density index $n < 1$, then the magnetic force term will be negative and this can be a justification for a decrease in outflow velocity value in proportion to the figures in Jiao & Wu (2011) (see figs 3 and 6 in Jiao & Wu 2011, for more details).

Fig. 3 shows the effect of various values of magnetic field parameter β_0 on the profiles of the physical variables. As stated before, β_0 is the ratio of gas to the magnetic pressure in the mid-plane of the disc. We adopt $\alpha = 0.1, \gamma = 5/3, f = 1, \eta = 0.1$ and $n = 0.85$. In this figure, the dotted, dashed and solid lines correspond to $\beta_0 = 10^4$, 10^3 and 10^2 respectively. The profiles of velocity components are shown in the top row of this figure. We see that on increasing the magnetic parameter β_0 in the equatorial plane of the disc, all three components of the velocity vector decrease towards the surface (notice that for a small value of β_0, a stronger magnetic field is present in the mid-plane of the disc). We therefore deduce that the velocity field reduces on enhancing the magnetic parameter β_0. Also, the thickness of the disc will decrease too. Moreover, according to the middle profiles of Fig. 3 it is predicted that the mass density and gas pressure decrease along the θ direction towards the surface of the disc. On the other hand, the magnetic pressure is enhanced and becomes strong near the surface of the disc on increasing β_0. Identical behaviour is shown in the profile of $b(\theta)$ in the bottom row of Fig. 3. Moreover, when we move towards the surface, the variation of magnetic field will reduce, as the initial condition is set in the equatorial plane and the value of this variable is considered equal to zero there. We thus show a negative value for the variation of magnetic field for all directions. As the behaviour of the gas and magnetic pressure are known, the ratio of these variables, i.e. $\beta(\theta)$, reduces along the θ direction from the equatorial plane to the surface of the disc.

One of the other important input parameters in our model is the magnetic diffusivity parameter, η_0, and its major behaviour has been shown in Fig. 4. The dotted, dashed and solid lines correspond to $\eta_0 = 0.1$, 0.2 and 0.3 respectively. We suppose that $\alpha = 0.1$, $\beta_0 = 10^3$, $f = 1$, $\gamma = 5/3$ and $n = 0.85$. The radial velocity and angular velocity will increase as η_0 increases, while the $v_\theta(\theta)$ component will be decreased. The parameter η_0 also increases, which is caused by a significant enhancement in the thickness of ADAFs. According to Fig. 4, we can see that magnetic pressure decreases with η_0. However, we are seeing an increase in magnetic pressure as the angle decreases and also on moving towards the disc

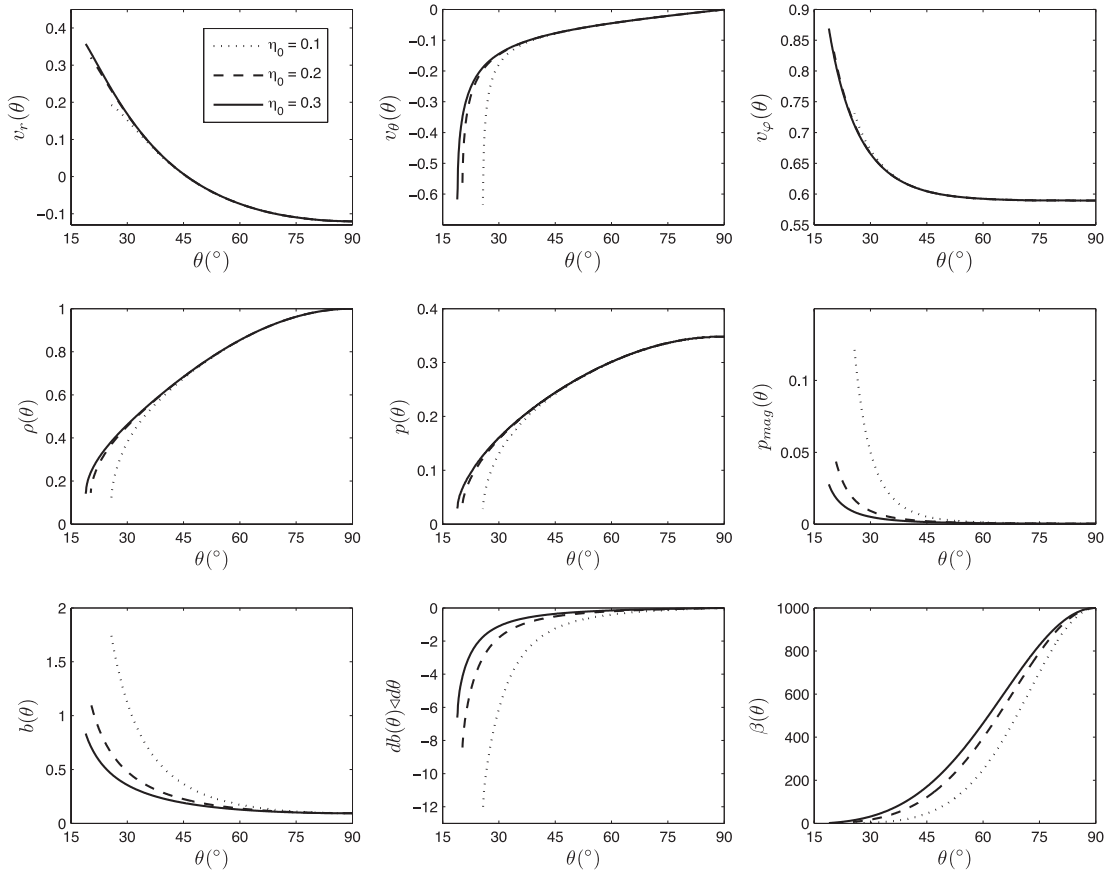

Figure 4. Profiles of the physical variables corresponding to the ADAF model along the θ direction for different values of magnetic diffusivity parameter, η_0. The dotted, dashed and solid lines denote $\eta_0 = 0.1, 0.2$ and 0.3 respectively. Here $\alpha = 0.1, \beta_0 = 10^3, f = 1, \gamma = 5/3$ and $n = 0.85$.

surface and approaching the vertical axis. The last row of Fig. 4 is dedicated to variations of the magnetic field and also the ratio of gas pressure to magnetic pressure. By looking at these figures, we can conclude that the η_0 parameter does not cause any shift in the inflow region; rather, it changes the outflow area. As a result, due to the symmetry considered in the equatorial plane previously mentioned, we can see an increase in magnetic field from the equatorial plane to the disc surface. The variation of magnetic field will increase with increasing η_0. Moreover, a decrease in the quantity $\beta(\theta)$ can be seen with decreasing angle, which reflects the fact that, while moving towards the disc, gas pressure is reduced and magnetic pressure increased and the result of this process of reduction in the value of $\beta(\theta)$ will be motion towards the vertical axis.

Another input parameter of the model is γ, which has been shown in Fig. 5. We assume that $\alpha = 0.1$, $\beta_0 = 10^3, f = 1$, $\eta_0 = 0.1$ and $n = 0.85$. As shown in Fig. 5, there is an increase of thickness with increasing γ parameter. The initial value of radial velocity at the equatorial plane reduces with γ and will actually be much more negative than before, which represents the inflow region increasing. Moreover, this parameter will make the $v_\theta(\theta)$ component of velocity negative and also will cause a significant reduction in the rotational speed of the accretion flow. According to the diagram, magnetic pressure and magnetic field are observed to increase with increasing parameter γ as the moving disc surface increases. Fig. 5 shows that variations in the field and the ratio of pressures will decrease as γ decreases.

On principle, this value must be smaller than unity in order not to violate the second law of thermodynamics. Fig. 6 shows fundamental variations in the quantity of discs with the parameters β_0, η_0, α and n in four separate panels. Fixed parameters corresponding to each of the graphs are listed at the top of each. The top left panel shows the ratio of outflow accretion over inflow accretion depending on different values of η_0 in the range $10^2 < \beta_0 < 10^4$. As previously mentioned, if β_0 decreases it shows the strong effect of magnetic field at the start point, i.e. in the equatorial plane. Then, according to this panel, it can be argued that reducing the magnetic field increases the proportion of discs. Also, this rate is smaller than unity, which indicates that most of the material increases towards the accretor and only a fraction of that moves out of the disc, finally leaving in the form of winds and jets. In the top right panel, the ratio of accretion rates to η_0 is also shown. A very interesting point in this diagram is that the η_0 parameter only increases at the outflow boundary and does not have a significant effect on inflow. Now, from this information it can be inferred that increasing the value of η_0 in the interval $0 < \eta_0 < 0.2$ has a dramatic effect, while in the interval $0.2 < \eta_0 < 1$ the behaviour of charts is fixed. The bottom left panel shows the behaviour of mass accretion rates with variation in viscosity parameter, α. We also considered the interval $0 < \alpha < 0.2$ for α, because it is in accord with observations. We see a dual behaviour of the viscosity parameter. In fact, at first we see the proportion of outflow ratio to inflow ratio. Around $\alpha = 0.05$, this increasing trend has stopped and in the interval $0.05 < \alpha < 0.2$

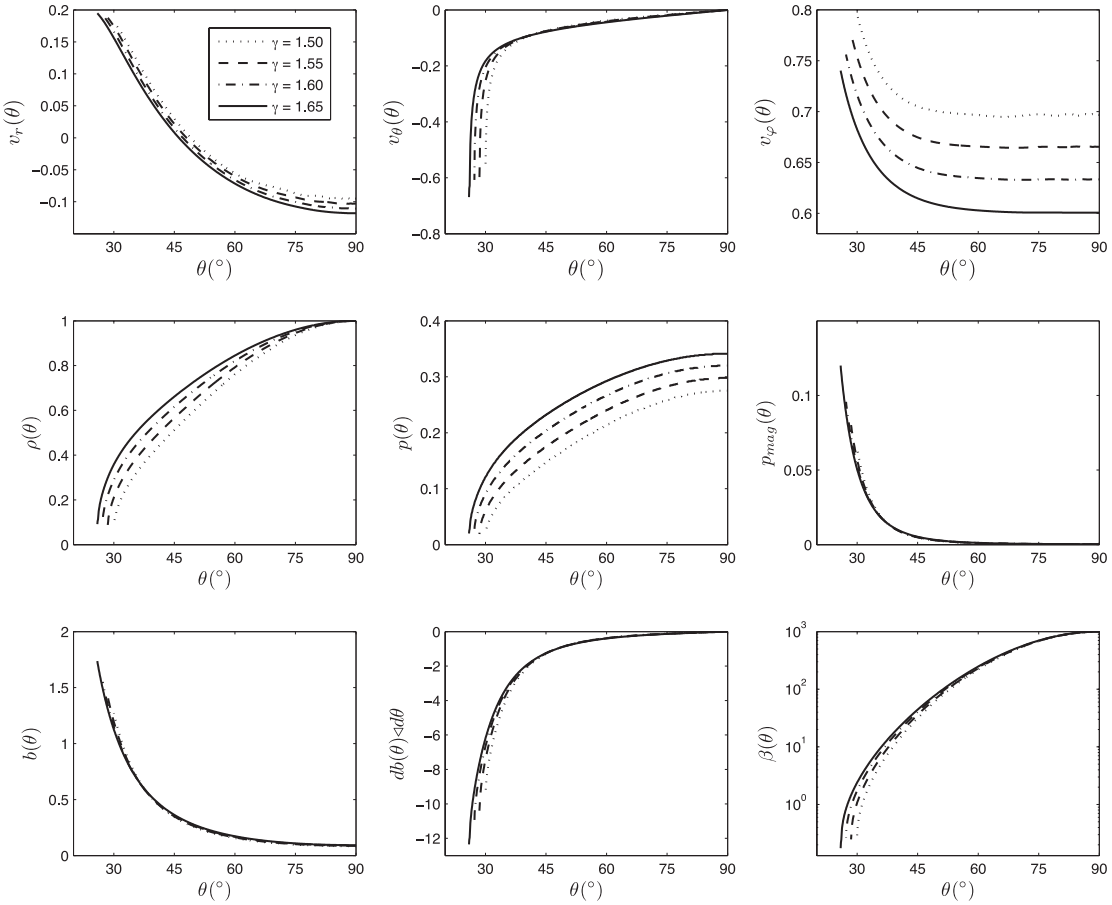

Figure 5. Profiles of the physical variables corresponding to the ADAF model along the θ direction for different values of the ratio of specific heats, γ. The dotted, dashed, dash–dotted and solid lines denote $\gamma = 1.50, 1.55, 1.60$ and 1.65 respectively. Here $\alpha = 0.1$, $\beta_0 = 10^3$, $f = 1$, $\eta_0 = 0.1$ and $n = 0.85$.

reduction in the diagram becomes apparent. As a result, we see a peak of the figure near $\alpha = 0.05$. This effect has also been seen by Jiao & Wu (2011) in their study of ADAFs (see their fig. 17, and for more information refer to their article). Finally, the bottom right of Fig. 6 shows the behaviour of the ratio of mass accretion rates to the variation of mass-density power-law index n. This can be understood by referring to previous figures, because we are seeing an increase in the ratio of outflow rate to inflow rate along n; then the mass density parameter, n, will increase at the outflow boundary, in perfect harmony with Fig 3. In accordance with the last simulation, we have considered a smaller range than the previous one, i.e. $0 < n < 1$. This increasing trend has also been observed in fig. 17 of Jiao & Wu (2011).

5 DISCUSSION

The main aim of this article is to verify the structure of advection-dominated accretion flows (ADAFs) along the θ direction when bathed in a toroidal magnetic field. The results have shown that the vertical structure of the disc is significantly affected by the magnetic field and its corresponding resistivity. By considering a self-similar solution along the radial direction, proper boundary conditions and reflection symmetry in the equatorial plane of the disc, we have constructed the structure of the disc along the θ direction explicitly. We have shown that only by assuming $v_\theta \neq 0$ do the solutions represent an inflow–outflow behaviour that is not reported in previous ADAF investigations. This assumption improved the solution of Narayan & Yi (1995a,b) to interpret the existence of outflows in hot accreting systems. Our disc consists of three different regions.

(1) The predominant region, called the inflow region. It extends from mid-plane to the place where the radial velocity is equal to zero, $v_r(\theta_0) = 0$, and contains the largest portion of the mass.
(2) An outflow region, which is located just after the inflow region and continues to the surface of the disc, in which matter starts escaping the central accretor in the r direction.
(3) The third region, called the wind region. This region contains material blowing out from the boundary of the outflow region. An area with very low width; since the self-similar solution has some drawbacks, we do not have much information about it.

Compared with the non-magnetic field solution (Jiao & Wu 2011), the existence of a magnetic field and its resistivity in our case can produce more advective energy. Also, the B-field configuration can affect energy transportation along accretion discs.

In this article we used two parameters β_0 and η_0 in order to study the effect of a magnetic field on the vertical structure of the disc. Our results showed that magnetic pressure will increase if θ changes on moving towards the surface of disc. Also, if we increase the β_0 parameter (which represents the ratio of gas pressure to field pressure at $\theta = 90^\circ$) it will enhance the rate of magnetic pressure growth (Fig. 3). Moreover, it was demonstrated that the disc's half-width declines as β_0 increases (Fig. 3).

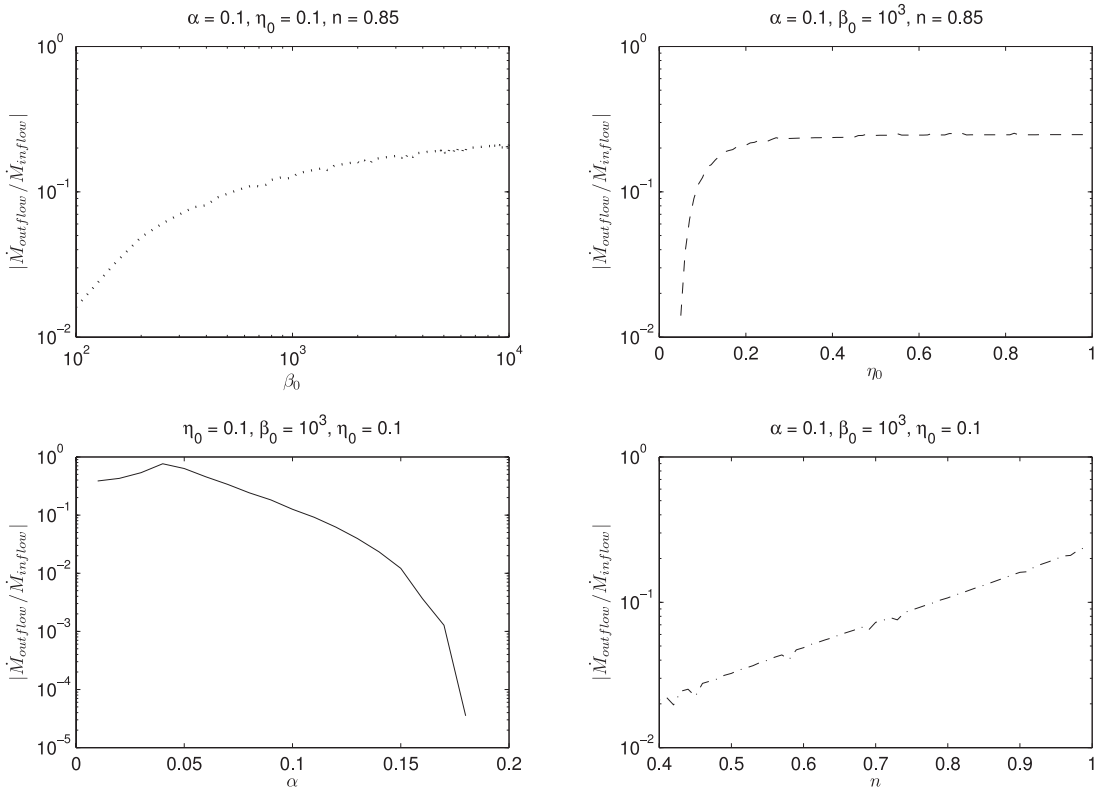

Figure 6. Profiles of the ratio of the outflow rate to the inflow rate corresponding to different input parameters: β_0, η_0, α and n. Here $\gamma = 5/3, f = 1$.

In a real accretion disc, there are several important processes other than viscosity and resistivity that we also expect to influence the dynamical structure of the disc, such as radiation pressure, photon trapping and any type of instability. It is immediately clear that changes in the boundary conditions affect the structure of the solutions and also it should be emphasized that we obtained this solution in a steady-state regime. Thus, the mere existence of a self-similar solution in no way guarantees that the solution is relevant to real accretion flows. Given these facts, the treatments in the article are very simplified; however, they are sufficiently general to describe many disc/outflow systems. Although we have made some simplifications in order to treat the problem analytically, the presented self-similar solutions show that the input parameters can significantly change the typical behaviour of the physical quantities of ADAF discs. Additionally, numerical simulations support the idea that the mass accretion rate, radial velocity and density can be well approximated as power laws (see e.g. Stone, Pringle & Begelman 1999; Yuan et al. 2012b). All these power-law profiles justify the self-similar methodology adopted in our work. Although the self-similar solutions are too simple to make any comparison with observations, we think that one may be able to relax the self-similarity assumptions and solve the equations of the model numerically. This kind of similarity solution could greatly facilitate testing and interpretation of the results.

ACKNOWLEDGEMENTS

We thank Fu-Guo Xie and Feng Yuan for their discussions and useful suggestions. We also appreciate the thoughtful and constructive comments of the referees, which clarified some points in the early version of the article.

REFERENCES

Abbassi S., Ghanbari J., Salehi F., 2006, A&A, 460, 357
Abbassi S., Ghanbari J., Najjar S., 2008, MNRAS, 388, 663
Abbassi S., Ghanbari J., Ghasemnezhad M., 2010, MNRAS, 409, 1113
Abbassi S., Nourbakhsh E., Shadmehri M., 2013, ApJ, 765, 96
Abramowicz M. A., Chen X., Kato S., Lasota J.-P., Regev O., 1995, ApJ, 438, L37
Akizuki C., Fukue J., 2006, PASJ, 58, 469
Bally J., Reipurth B., Davis C. J., 2007, in Reipurth B., Jewitt D., Keil K., eds, Protostars and Planets V. Univ. Arizona Press, Tucson, p. 215
Beckwith K., Hawley J. F., Krolik J. H., 2009, ApJ, 707, 428
Blandford R., Begelman M., 1999, MNRAS, 303, L1
Blandford R., Begelman M., 2004, MNRAS, 349, 68
Blandford R. D., Payne D. G., 1982, MNRAS, 199, 883
Bu D., Yuan F., Xie F., 2009, MNRAS, 392, 325
De Villiers J. P., Hawley J. F., Krolik J. H., 2003, ApJ, 599, 1238
De Villiers J.-P., Hawley J. F., Krolik J. H., Hirose S., 2005, ApJ, 620, 878
Dionatos O. et al., 2009, ApJ, 692, 1
Dionatos O., Nisini B., Cabrit S., Kristensen L., Pineau Des Forets G., 2010, A&A, 521, A7
Esin A. A., Narayan R., Ostriker E., Yi I., 1996, ApJ, 465, 312
Ghanbari J., Salehi F., Abbassi S., 2007, MNRAS, 381, 159
Gorti U., Hollenbach D., 2009, ApJ, 690, 1539
Hameury J. M., Lasota J. P., Maclintock J. E., Narayan R., 1997, ApJ, 489, 234
Ichimaru S., 1977, ApJ, 214, 840
Jiao C. L., Wu X. B., 2011, ApJ, 733, 112
Kaburaki O., 2000, ApJ, 531, 210
Kato S., Fukue J., Mineshige S., 2008, Black Hole Accretion Discs: Towards a New Paradighm. Kyoto Univ. Press, Kyoto
Manmoto T., Kato S., Nakamura K., Narayan R., 2000, ApJ, 529, 127
Mckinney J., Tchekhovskoy A., Blandford R., 2012, MNRAS, 423, 3083

Mosallanezhad A., Khajavi M., Abbassi S., 2013, Res. Astron. Astrophys., 13, 87
Narayan R., Yi I., 1994, ApJ, 428, L13
Narayan R., Yi I., 1995a, ApJ, 444, 238
Narayan R., Yi I., 1995b, ApJ, 452, 710
Narayan R., Maclintock J. E., Yi I., 1996, ApJ, 457, 821
Narayan R., Kato S., Honma F., 1997, ApJ, 476, 49
Narayan R., Igumenshchev I. V., Abramowicz M. A., 2000, ApJ, 539, 798
Ohsuga K., Mineshige S., 2011, ApJ, 736, 1
Okuda T., Teresi V., Toscano E., Molteni D., 2005, MNRAS, 357, 295
Pen U.-L., Matzener C. D., Wong S., 2003, ApJ, 596, L207
Piran T., 1977, MNRAS, 180, 45
Pudritz R. E., 1985, ApJ, 293, 216
Quataert E., Gruzinov A., 2000, ApJ, 539, 809
Rees M. J., Begelman M. C., Blandford R. D., Phinney E. S., 1982, Nature, 295, 17
Shadmehri M., Khajenabi F., 2005, MNRAS, 361, 719
Shakura N. I., Sunyaev R. A., 1973, A&A, 24, 337
Shapiro S. L., Lightman A. P., Eardley D. M., 1976, ApJ, 204, 187
Stone J. M., Pringle J. E., 2001, MNRAS, 322, 461
Stone J. M., Pringle J. E., Begelman M. C., 1999, MNRAS, 310, 1002
Takahara F., Rosner R., Kusunose M., 1989, ApJ, 346, 122
Whelan E. T. et al., 2005, Nature, 435, 652
Xie F., Yuan F., 2008, ApJ, 681, 499
Xie F., Yuan F., 2012, MNRAS, 427, 1580
Xue L., Wang J.-C., 2005, ApJ, 623, 372
Yuan F., 2001, MNRAS, 324, 119
Yuan F., Bu D., 2010, MNRAS, 408, 1051
Yuan F., Quataert E., Narayan R., 2003, ApJ, 598, 301
Yuan F., Quataert E., Narayan R., 2004, ApJ, 606, 894
Yuan F., Wu M., Bu D., 2012a, ApJ, 761, 129 (I)
Yuan F., Bu D., Wu M., 2012b, ApJ, 761, 130 (II)

This paper has been typeset from a TEX/LATEX file prepared by the author.